

# Reevaluating the $a_1(1420)$ enhancement and its molecular partners in the low-lying axial-vector meson spectrum

Mao-Jun Yan,<sup>1,\*</sup> Chun-Sheng An,<sup>1</sup> and Cheng-Rong Deng<sup>1</sup>

<sup>1</sup>*School of Physical Science and Technology, Southwest University, Chongqing 400715, China*

(Dated: December 3, 2025)

We assess possible axial-vector states with  $G$ -parity ( $G = \pm 1$ ) dynamically generated by pseudoscalar-vector interactions in coupled channels, driven by the Weinberg-Tomozawa term at leading order in chiral perturbation theory. The  $S$ -wave amplitudes are unitarized via the Bethe-Salpeter equation, and poles of the unitarized amplitudes are searched for in the complex energy plane. In the isovector sector with  $I^G(J^{PC}) = 1^\pm(1^{+\mp})$ , we identify two poles around 1400 MeV in the second Riemann sheet below the  $K^*\bar{K}$  mass threshold. The  $G = +1$  and  $G = -1$  poles can be one of the origins of the peaks in the  $f_0(980)\pi$  and  $\phi\pi^0$  mass spectra reported by the COMPASS and BESIII collaborations, respectively, in the  $\pi N \rightarrow \pi\pi\pi N$  and  $J/\psi \rightarrow \eta\phi\pi$  processes, in addition to triangle singularity effects discussed in the literature. Additionally, the poles in the isoscalar sector may explain the nontrivial behavior of the  $K^*\bar{K}$  spectra line shapes measured by several experiments in different reactions. Specifically, for the  $0^+(1^{++})$  case, we find a sizeable  $K^*\bar{K}$  component for the  $f_1(1420)$ . In the  $0^-(1^{+-})$  scenario, the pole strongly coupled to  $\rho\pi$  can be associated with the  $h_1(1170)$  resonance. Lastly, in this same sector, we identify a higher pole that dominates the  $K^*\bar{K}$  invariant mass in the  $\chi_{cJ} \rightarrow \phi K^*\bar{K}$  decay, where the  $h_1(1415)$  is observed in the BESIII data.

arXiv:2512.02655v1 [hep-ph] 2 Dec 2025

---

\* [yanmj0789@swu.edu.cn](mailto:yanmj0789@swu.edu.cn)

## I. INTRODUCTION

Thanks to the increased technological power in experimental particle physics over the past two decades, we are witnessing unprecedented development in hadron physics. Since 2003, an ever-growing number of new hadronic states have been observed. These states possess features that are challenging to explain using the conventional quark model for quark-antiquark mesons and three-quark baryons, and thus candidates of exotic hadrons (see the reviews [1–12]).

Unlike the heavy sector, where we have clear evidence of exotic hadrons such as, the  $Z_c(3900)^\pm$  [13, 14], evidence is not as compelling in the light quark sector. A recent example in this sector is the newly structure  $\eta_1(1855)$ , observed by the BESIII in the reaction  $J/\psi \rightarrow \gamma\eta\eta'$  [15, 16]. Its most probable quantum numbers are  $J^{PC} = 1^{-+}$ , which are essentially exotic, given that such a combination cannot be obtained from the  $q\bar{q}$  one. Although intense theoretical activity discusses the most probable configuration for the  $\eta_1(1855)$  structure, there is still no consensus regarding which quark structure is the most appropriate [17–24].

Another very interesting example is the case of the  $a_1(1420)$  structure observed in the COMPASS experiment [25], in the reaction  $\pi N \rightarrow \pi\pi\pi + N$ , that is, in the diffractive process of dissociation of a 190 GeV pion beam interacting with a stationary hydrogen target, which, upon interaction with an emitted pomeron by the proton target, gets excited, producing a resonant structure that decays into a final state of pions. In particular, the  $a_1(1420)$  structure is claimed by COMPASS upon finding a peak around  $1414_{-13}^{+15}$  MeV and width  $\Gamma \simeq 153_{-23}^{+8}$  MeV [25], in the distribution for  $f_0(980)\pi$  ( $f_0(980) \rightarrow \pi^+\pi^-$ ). Initially claimed as a new meson, the  $a_1(1420)$  structure is subsequently suggested to be a triangle singularity (TS) effect of the  $K^*\bar{K}K$  loop diagram [26–29]. In other words, the peak observed in the  $f_0(980)\pi$  spectrum by COMPASS is assigned to be a TS effect, resulting from the decay of the  $a_1(1260)$  state into  $K^*\bar{K}$ , and then  $K^*$  into  $K\pi$ , with the final  $K\bar{K}$  pair of mesons merging to give rise the  $f_0(980)$ . However, recent data from the Belle collaboration [30] in  $\tau^- \rightarrow \pi^-\pi^-\pi^+\nu_\tau$  decay seem to indicate a new direction in interpreting the  $a_1(1420)$  structure. On the one hand, the  $\tau^- \rightarrow \pi^-\pi^-\pi^+\nu_\tau$  predominantly proceeds through  $a_1(1260)$  resonance [30], which then decays into the  $\rho\pi$ , with  $\rho \rightarrow \pi\pi$ . On the other hand, the  $a_1(1420)$  resonance is seen at the COMPASS experiment in the  $3\pi$  distribution as well. Like the  $a_1(1260)$ , the  $a_1(1420)$  is an axial-vector with  $1^{++}$  quantum numbers, and if it indeed exists, it should also manifest in the pion spectrum from  $\tau^- \rightarrow \pi^-\pi^-\pi^+\nu_\tau$  data. Thus, by performing a partial-wave analysis on the  $\tau^- \rightarrow \pi^-\pi^-\pi^+\nu_\tau$  decay data, the Belle collaboration found a signal corresponding to the  $a_1(1420)$  state. The mass  $1387.8 \pm 0.3$  MeV and width

$109.2 \pm 0.6$  MeV are both slightly smaller than those measured by COMPASS, which could be due to a coherent background in COMPASS that dominates the  $3\pi$  low-mass region. Undoubtedly, the new measurements provided in Ref. [30] further drive the discussion regarding the nature of the  $a_1(1420)$  structure, such that interpretations different from solely a TS effect [27–29] cannot be ruled out.

A similar situation is encountered in the  $J/\psi \rightarrow \eta\phi\pi^0$  decay, measured by the BESIII experiment [31]. In particular, we can observe an accumulation of events around 1400 MeV in the distribution of the  $\phi\pi^0$  pair in the Dalitz plot [31], which, when projected onto the corresponding invariant mass, corresponds to a peak near the  $K^*\bar{K}$  mass threshold, which, in principle, could be associated with a  $C = -1$  hadronic state or, as pointed out in Ref. [32], could be a kinematic effect due to a TS. Recently, in a new study by BESIII [33] on  $J/\psi \rightarrow \eta\phi\pi^0$  decays, the prominent peak in the  $\phi\pi^0$  spectrum at around 1400 MeV is explained as a non- $\phi$  background contribution. In summary, in the case of the  $a_1(1420)$  and the signal observed by BESIII, we are facing an intriguing situation where interpretations as a TS or a genuine hadronic state both seem to account for the same data.

In both cases discussed above, the enhancements show up near the  $K^*\bar{K}$  threshold and, in principle, we might think that such observations could be explained as dynamically generated states from  $K^*\bar{K}$  interaction. Such an approach is utilized in Ref. [34], where the single-channel  $K\bar{K}^*$  interaction is studied using the chiral unitary approach (ChUA) [35–39]. However, the dynamically generated states as given in Ref. [34] do not correspond to any of the resonant structures around 1400 MeV discussed above, i.e., we cannot assign them to the  $a_1(1420)$  state observed by COMPASS [25] or to the enhancement in the  $\phi\pi^0$  spectrum observed by BESIII [31, 33]. It is worth noting that the studies in Ref. [34] do not include searches for virtual-state-like poles in the solution of the unitarized  $T$ -matrix via the Bethe-Salpeter equation. By virtual-state-like poles, we mean, in the case at hand, poles below the  $K^*\bar{K}$  mass threshold in the complex energy ( $\sqrt{s}$ ) plane on the unphysical Riemann sheet with respect to the  $K^*\bar{K}$  cut (where the  $K^*$  width is neglected), while bound-state-like poles appear as also below the  $K^*\bar{K}$  threshold but on the physical Riemann sheet.

With this in mind, we aim to investigate the pseudoscalar-vector ( $PV$ ) interactions, described at leading-order in the chiral expansion by a Weinberg-Tomozawa (WT) term and unitarized via the Bethe-Salpeter equation, following ChUA. Consequently, we will show, in particular, that the  $a_1(1420)$  state observed by COMPASS [25], initially claimed as a new meson and later interpreted as a TS in Refs. [27–29], can also be explained by a virtual-state-like pole resulting mainly from the  $K^*\bar{K}$  interaction though additional TS effects may also play a pole. To support this claim, we calculate the distribution and compare it with the corresponding COMPASS data. Although our

model appears much simpler than the one proposed by Ref. [29], which attributes the COMPASS observation to a TS effect, it matches the data well across the distribution range, particularly around 1400 MeV.

Additionally, we will investigate the isovector sector with negative G-parity, where the experimental  $b_1(1235)$  state [40] is a member of the  $I^G(J^{PC}) = 1^-(1^{+-})$  multiplet. We also find a virtual-state-like pole around 1400 MeV, named  $b_1(1400)$ . Interestingly, a signal appears precisely in this energy region in the  $\phi\pi^0$  spectra from the BESIII analysis of the  $J/\psi \rightarrow \eta\phi\pi^0$  decay [31, 33], which is assigned to a non- $\phi$  background contribution in the BESIII analysis [33].

Besides the isovector sector, the ChUA is used to further explore the  $PV$  interactions in the isoscalar sector. Experimentally, two observed states exist for each sign of G-parity in this sector. For  $G = +1$ , the states are  $f_1(1285)$  and  $f_1(1420)$ , and for  $G = -1$ , they are  $h_1(1170)$  and  $h_1(1415)$  [40]. Comparison with experimental data suggests identifying the  $f_1(1420)$  as having a sizable  $K^*\bar{K}$  component. Meanwhile, the  $h_1(1170)$  and  $h_1(1415)$  can be identified in our findings with poles that couple strongly to  $\rho\pi$  and  $K^*\bar{K}$ , respectively.

This article is structured as follows. In Section II, we briefly discuss the main points of ChUA, explicitly presenting the WT term for the  $S$ -wave  $PV$  interactions. In Section III, we discuss the relevant isovector channels contributing to the  $PV$  interactions in the energy region of our interest. We also show how our findings manifest in the corresponding line shapes of the  $f_0(980)\pi$  and  $\phi\pi^0$  spectra, as measured by the COMPASS and BESIII experiments. In Section IV, we turn to the isoscalar spectrum and discuss our findings for both positive and negative G-parity sectors. The well-known double-pole structure assigned to  $K_1(1270)$  is briefly discussed in Section V, where we examine the influence of the nonzero width of  $K^*$  meson on the line shape of the modulus squared of the corresponding  $T$ -matrix elements. Finally, a summary is provided in Section VI.

## II. PSEUDOSCALAR-VECTOR MESONS SCATTERING

The  $S$ -wave interaction among pseudoscalar and vector mesons given by the WT term reads [34]

$$V_{ij}(s) = \frac{\epsilon \cdot \epsilon'}{8F_\pi^2} C_{ij} \left[ 3s - (M^2 + m^2 + M'^2 + m'^2) - \frac{1}{s}(M^2 - m^2)(M'^2 - m'^2) \right], \quad (1)$$

where the index  $i(j)$  stands for the initial (final)  $PV$  channel, while  $F_\pi$  corresponds to the pion decay constant ( $\simeq 92.1$  MeV), and  $\epsilon(\epsilon')$  is the four-vector polarization of the incoming (outgoing) vector meson. Additionally, we denote  $M(M')$ , and  $m(m')$  as the masses for the initial (final) vector and pseudoscalar mesons, respectively. The  $C_{ij}$  coefficients have been given in Ref. [34].

Within ChUA, all transitions from the  $i$ -th to the  $j$ -th channel are unitarized using the Bethe-Salpeter equation in coupled channels. This equation, in its on-shell factorization form, is expressed as [37]

$$T = (1 - VG)^{-1}V, \quad (2)$$

where  $V$  represents the kernel matrix, whose elements are determined by Eq. (1) above. Meanwhile,  $G$  is the diagonal matrix with elements  $G_\ell$  corresponding to the loop function for the  $\ell$ -th  $PV$  channel. On the one hand, given that  $G_\ell$  is ultraviolet (UV) divergent, it can be regularized by introducing a cutoff in the three-momentum  $q_{\max}$ , such that

$$\begin{aligned} G_\ell &= i \int \frac{d^4q}{(2\pi)^4} \frac{1}{q^2 - m_\ell^2 + i\epsilon} \frac{1}{(q - P)^2 - M_\ell^2 + i\epsilon}, \\ &= \int_{|\mathbf{q}| < q_{\max}} \frac{d^3q}{(2\pi)^3} \frac{\omega_1(\mathbf{q}) + \omega_2(\mathbf{q})}{2\omega_1(\mathbf{q})\omega_2(\mathbf{q})} \frac{1}{(P^0)^2 - (\omega_1(\mathbf{q}) + \omega_2(\mathbf{q}))^2 + i\epsilon}, \end{aligned} \quad (3)$$

where  $\omega_1(\mathbf{q}) = \sqrt{M_\ell^2 + |\mathbf{q}|^2}$  and  $\omega_2(\mathbf{q}) = \sqrt{m_\ell^2 + |\mathbf{q}|^2}$ . Here,  $m_\ell$  and  $M_\ell$  represent the masses of the pseudoscalar and vector mesons, respectively, involved in the loop in the channel  $\ell$ , and  $P$  the total four-momentum of those mesons ( $P^2 = s$ ). On the other hand, we can also adopt the dimensional regularization scheme to deal with the UV divergence. In this case, the loop-function assumes the following form [38, 41]

$$\begin{aligned} G_\ell^{\text{DR}}(s) &= \frac{1}{16\pi^2} \left[ \alpha_\ell(\mu) + \log \frac{M_\ell^2}{\mu^2} + \frac{m_\ell^2 - M_\ell^2 + s}{2s} \log \frac{m_\ell^2}{M_\ell^2} \right. \\ &\quad \left. + \frac{p_\ell}{\sqrt{s}} \left( \log \frac{s - m_\ell^2 + M_\ell^2 + 2p_\ell\sqrt{s}}{-s + m_\ell^2 - M_\ell^2 + 2p_\ell\sqrt{s}} + \log \frac{s + m_\ell^2 - M_\ell^2 + 2p_\ell\sqrt{s}}{-s - m_\ell^2 + M_\ell^2 + 2p_\ell\sqrt{s}} \right) \right], \end{aligned} \quad (4)$$

where  $\alpha_\ell(\mu)$  is a subtraction constant that absorbs any changes in the scale of the regularization, denoted by  $\mu$ , and  $p_\ell$  corresponds to the three-momentum of the mesons in the center-of-mass (c.m.) frame, given by

$$p_\ell = \frac{1}{2\sqrt{s}} \sqrt{\left(s - (M_\ell + m_\ell)^2\right) \left(s - (M_\ell - m_\ell)^2\right)}. \quad (5)$$

In this work, we set  $\mu = 1000$  MeV. Furthermore, the subtraction constant  $\alpha_\ell(\mu)$  for each  $PV$  loop is obtained by matching Eqs. (3) and (4) at the corresponding  $PV$  threshold.

In order to search for poles in the  $T$ -matrix, we look at its solutions on the energy complex plane. As a result, we should address the interplay of the different Riemann sheets stemming from the branch cut in the  $G_\ell$  loop function. For instance, there are two Riemann sheets for a single-channel system. In this case, the poles that show up below threshold on the real energy axis on the first (physical) Riemann sheet correspond to bound states. The poles corresponding to virtual

states are located below threshold on the real energy axis but on the second (unphysical) Riemann sheet. Also on the second Riemann sheet are resonances, which are poles off the real energy axis. Thus, denoting  $G_\ell^{\text{I}}(s)$  and  $G_\ell^{\text{II}}(s)$  as the loop-functions in the first and second Riemann sheets, respectively, we have

$$G_\ell^{\text{II}}(s) = G_\ell^{\text{I}}(s) + i \frac{p_\ell}{4\pi\sqrt{s}}. \quad (6)$$

### III. ISOVECTOR SPECTRUM

#### A. $a_1(1260)$ and $a_1(1420)$

In this case, we consider two channels, namely:  $\rho\pi$  and  $K^*\bar{K}$ . In Table I, we list the coefficients  $C_{ij}$  of the WT terms in Eq. (1) corresponding to the transitions between the aforementioned channels. Note that, from Table I, both diagonal transitions of  $K^*\bar{K}$  are attractive, which may imply poles in the solution of Eq. (2). In particular, we can anticipate the existence of poles in our study given the similarity between the WT terms, especially for the  $K^*\bar{K}$  channel, and those of the  $N\bar{K}$  and  $K_1\bar{K}$  interactions, studied in Refs. [22, 42], which resulted in states attributed to the structures  $\Sigma(1440)$  and  $\pi_1(1600)$ , respectively. It is worth mentioning that the  $K^*\bar{K}$  interaction is previously investigated within ChUA in Ref. [34]. However, the authors ignore whether the interaction could result in states associated with virtual-state-like poles in the solution of Eq. (2). As discussed earlier, such poles manifest themselves below the threshold on the second Riemann sheet in the complex energy plane.

TABLE I.  $C_{ij}$  coefficients in isospin basis for  $S = 0, I = 1$ .

$a_1$	$\rho\pi$	$K^*\bar{K}$
$\rho\pi$	-2	$\sqrt{2}$
$K^*\bar{K}$	$\sqrt{2}$	-1

We work in the isospin symmetric basis, and label channels  $\rho\pi$  and  $K^*\bar{K}$  (with negative  $G$  parity) as channels 1 and 2, respectively. We label the Riemann sheets in this system as  $\text{RS}_{\pm\pm}$ , where the first and second subindices denote the signs of  $\text{Im}q_1$  and  $\text{Im}q_2$ , with  $q_1$  and  $q_2$  the c.m. momenta in the two channels. In the coupled-channel amplitudes with switching off the  $\rho\pi - K^*\bar{K}$  transition, we find poles located at  $\sqrt{s_p} = 1336 - i 130$  MeV using  $q_{\text{max}} = 800$  MeV, and at  $\sqrt{s_p} = 1331 - i 77$  MeV for  $q_{\text{max}} = 1000$  MeV on  $\text{RS}_{--}$ .

To study the location of the higher pole in the  $\rho\pi - K^*\bar{K}$  scattering, the  $C_{ij} = \sqrt{2}$ , in Table I, is reparameterized as  $x\sqrt{2}$ , where the corresponded poles on  $RS_{--}$  are shown in Figs. 1 and 2. As  $x$  increases, the pole becomes broader and farther away from the  $K^*\bar{K}$  threshold. Especially, when the  $x$  closes to 1, the pole position changes rapidly, where the effective potential in elastic  $K^*\bar{K}$  scattering is reduced to be negligible. This type of divergent trajectory of the poles suggests that the on-shell approximation may not be applicable in this process.

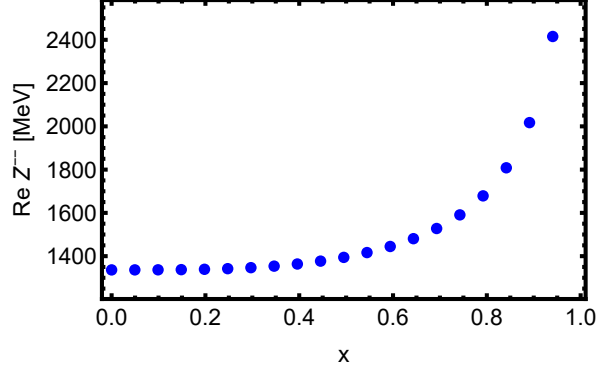


FIG. 1. The real parts of the poles on  $RS_{--}$  corresponding to the subtractions matched to  $q_{max} = 800$  MeV.

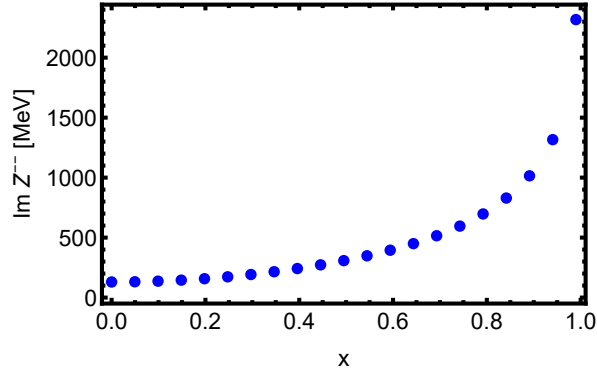


FIG. 2. The imaginary parts of the poles on  $RS_{--}$  corresponding to the subtractions matched to  $q_{max} = 800$  MeV .

In the case of  $V_{11}V_{22} \simeq V_{12}^2$ , the determinant of T-matrix reads

$$(1 - V_{11}G_{11})(1 - V_{22}G_{22}) - V_{12}^2G_{11}G_{22} \simeq 1 - V_{11}G_{11} - V_{22}G_{22}, \quad (7)$$

which reduces to a single-channel-like process with only one pole that can be solved numerically. Concerning the  $V_{11}/V_{22} = 29.17$  at  $\rho\pi$  threshold, a pole of T-matrix is from  $1 - V_{11}G_{11} = 0$ , which is consistent with the study in Ref. [34].

To pin down the ambiguity from the on-shell approximation in the coupled channel scattering, the one-loop correction is evaluated without introducing the on-shell approximation,

$$\overline{VG} = \frac{\epsilon \cdot \epsilon'}{4F_\pi^2} \int \frac{d^4l}{(2\pi)^4} \frac{(p+p-l)_\mu (q+l)^\mu}{(p-l)^2 - M^2} \frac{1}{l^2 - m^2} = \frac{\epsilon \cdot \epsilon'}{4F_\pi^2} \int \frac{d^4l}{(2\pi)^4} \frac{\tilde{N}}{f(l)}, \quad (8)$$

where the momentum of the incoming (outgoing) pseudoscalar meson in V are  $q$  and  $l$ , respectively.

The numerator of the integrand reads

$$\tilde{N} = 2p^\mu q_\mu + 2p^\mu l_\mu + (q^2 - l^2). \quad (9)$$

The first term on the right-hand side of Eq. (9) is independent of the loop momentum  $l$ . The second term contains  $2p^0 l^0$  and  $2\vec{p} \cdot \vec{l}$ , the former of which is an odd function of the  $l^0$  and vanishes after integration over  $l^0$  from  $-\infty$  to  $\infty$ . Concerning the spherical angle between  $\vec{p}$  and  $\vec{l}$ ,  $2\vec{p} \cdot \vec{l}$  turns out to be zero after S-wave projection. For the third term, the  $l^2$  leads to UV divergence in the integral, and the divergent part is absorbed into the higher-order interaction in the chiral perturbation theory, where the integrations over  $l^0$  and  $\vec{l}$  correspond to the next-to-leading order (NLO) and the next-to-next-to-leading order (NNLO), respectively. The finite part of the NLO corresponds to the on-shell meson and its upper limit is evaluated with the  $l^0, 2$  in the  $\tilde{N}$  approached by a constant  $q_{max}^2 + m_{i,j}^2$ . One of the NNLO is ignored, which implies  $\overline{VG} \simeq \mathcal{O}(10^{-1}) VG$  in the window of 1300 – 1450 MeV, where the iteration in the one-loop order is negligible. Consequently, the correction from the inelastic scattering is small and agrees with the argument on kinematical suppression in coupled channel scattering with a large mass difference between thresholds. The higher pole in the  $\rho\pi - K^*\bar{K}$  scattering behaves as the solutions, with a small  $x \leq 0.1$ , in Figs. 1 and 2.

Being shielded by the  $K^*\bar{K}$  threshold, these poles manifest as threshold cusps in the line shape of the  $T$ -matrix elements. In Fig. 3, we can see the line shapes of the modulus squared of the  $T$ -matrix elements corresponding to the diagonal transitions  $\rho\pi \rightarrow \rho\pi$ , and  $K^*\bar{K} \rightarrow K^*\bar{K}$ , denoted in Fig. 3 by  $T_{11}$  and  $T_{22}$ , respectively. Specifically for the  $K^*\bar{K} \rightarrow K^*\bar{K}$  transition, we note a sharply pronounced cusp structure (blue dashed line) at the  $K^*\bar{K}$  threshold, where the sharpness depends on the distance of the pole to the threshold [43].

On the other hand, when we include in our formalism the contribution due to the finite width of the  $\rho$  and  $K^*$  vector mesons, we now observe that the cusp structure seen previously smoothens, transforming into a broad and asymmetric peak, shifted to the region around 1420 MeV (blue solid line), close to the mass of the structure  $a_1(1420)$  reported by COMPASS in Ref. [25].

In both cases, with and without the inclusion of the widths of the vector mesons, the manifestation of the pole is visible, generated from the dynamics of the  $K^*\bar{K}$  interaction, notably in the

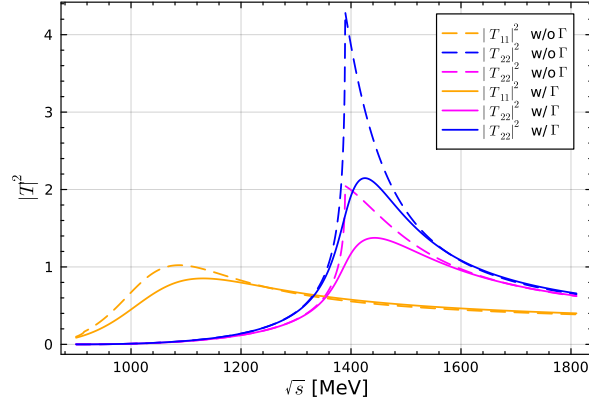


FIG. 3. Modulus squared of  $T$ -matrix elements. The dashed and solid lines correspond to the solutions of Eq. (2), considering the vector meson width as zero and finite, respectively. The orange and blue lines are  $|T_{11}|^2$  and  $|T_{22}|^2$  determined by choosing a subtraction constant for the loops involved, matching Eqs. (3) and (4) at threshold with  $q_{\max} = 1000$  MeV, while the magenta lines are  $|T_{22}|^2$  determined with  $q_{\max} = 800$  MeV.

mass region of the  $a_1(1420)$  structure. Thus, it is plausible that the  $a_1(1420)$  structure reported by COMPASS receives an important contribution from the above pole, in addition to the TS contribution discussed in Refs. [27–29]. In this case, we do not find any signal that could be attributed to the structure  $a_1(1420)$ , which is consistent with the observations from COMPASS [44] since no signal of  $a_1(1420)$  is observed in the  $\rho\pi$  distribution.

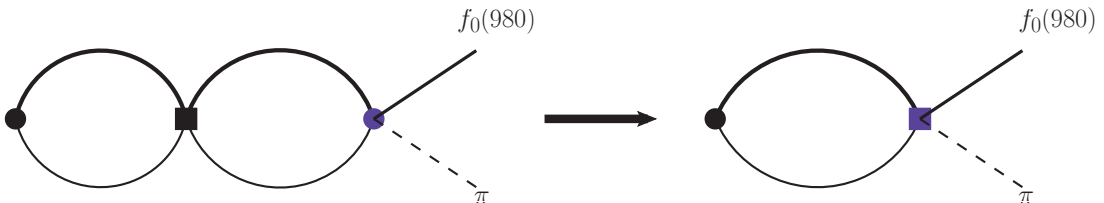


FIG. 4. The  $K^*\bar{K}$  transition to  $f_0(980)\pi$  via final state interaction. The black dot and rectangle represent the  $K^*\bar{K}$  production rate and the unitarized scattering amplitude, respectively. The bold, solid, and dashed lines represent the vector mesons, kaon, and pion, respectively. The solid dot and rectangle indicate the production vertex of  $K^*\bar{K}$  and the coupled channel scattering amplitude. The blue vertices represent the effective  $K^*\bar{K} \rightarrow f_0(980)\pi$  transition, including the  $K^*\bar{K} \rightarrow \rho\pi$  coupled channel scattering.

We can test this hypothesis by calculating the differential cross section  $d\sigma/dM_{\text{inv}}$  as a function of the invariant mass of the  $f_0(980)\pi$  pair and comparing it with the corresponding COMPASS data. Consider the Feynman diagram illustrated in Fig. 4 for this task. In particular, the corresponding amplitude can be written as

$$N \tilde{G}_{K^*\bar{K}} T_{K^*\bar{K} \rightarrow f_0\pi}, \quad (10)$$

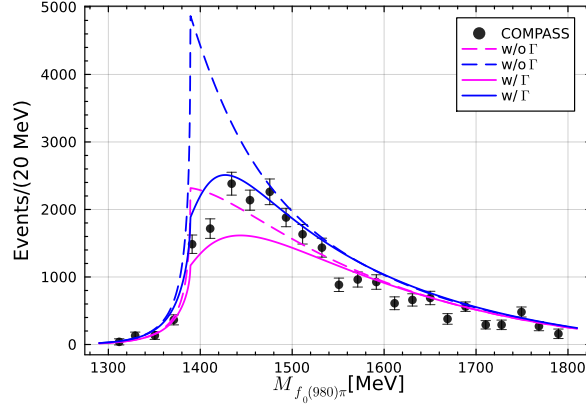


FIG. 5. Numerical results for Eq. (12) corresponding to the  $f_0(980)\pi$  invariant mass distribution compared to the data from COMPASS [29]. The subtraction constant regularizing the loop associated with the production is  $\alpha(\mu = 1000 \text{ MeV}) = -0.70$ .

where  $N$  parameterizes the production of the  $K^*\bar{K}$  pair, while  $\tilde{G}_{K^*\bar{K}}$  represents the loop of the  $K^*$  and  $\bar{K}$  mesons, given by Eq. (3), where the subtraction constant, in this case, will be obtained by tuning our results to data. Notice that the loop functions  $\tilde{G}_{K^*\bar{K}}$  and  $G_{K^*\bar{K}}$  are associated with the production and poles in the T-matrix, respectively, where the dynamics in the short distances are different, and the truncations in the loop functions are not correlated. Furthermore, the matrix element  $T_{K^*\bar{K} \rightarrow f_0\pi}$  associated with the effective transition is encoded by the parameter  $P_{a_1}$  also to be constrained by matching, such that

$$T_{K^*\bar{K} \rightarrow f_0\pi} = P_{a_1} T_{K^*\bar{K} \rightarrow K^*\bar{K}} |\vec{q}_\pi|, \quad (11)$$

where  $|\vec{q}_\pi|$  corresponds to the magnitude of the outgoing pion momentum in the  $f_0\pi$  c.m. frame. Therefore, the differential cross section  $d\sigma/dM_{\text{inv}}$  is given by

$$\frac{d\sigma}{dM_{\text{inv}}} = \frac{|\vec{q}_\pi|}{8\pi M_{\text{inv}}} |\mathcal{M}|^2, \quad (12)$$

with  $\mathcal{M}$  given by Eq. (10).

In Fig. 5, we show the line shape from Eq. (12), compared with the COMPASS data. The data are well described by using the subtraction constant  $\alpha(\mu = 1000 \text{ MeV}) = -0.70$  (correspondingly, the cutoff  $q_{\text{max}}$  matched at the  $K^*\bar{K}$  threshold is 660 MeV). In particular, the asymmetric line shape is naturally reproduced by our model.

In the  $\rho\pi \rightarrow \rho\pi$  transition in Fig. 3 (dashed orange line), if we move to the low-energy part in Fig. 3, we notice, for the case of zero-width of the vector mesons, a pronounced bump around 1100 MeV, which is far away from the  $\rho\pi$  mass threshold. Indeed, we expect that such a nontrivial

structure could show up in this case since the corresponding  $C_{ij}$  absolute value for  $\rho\pi$  is larger than that for  $K^*\bar{K}$  in Table I. Correspondingly, we find poles at for  $\sqrt{s_p} = 1019 - i 126$  MeV using  $q_{\max} = 800$  MeV, and at  $\sqrt{s_p} = 998 - i 99$  MeV for  $q_{\max} = 1000$  MeV on  $\text{RS}_{-+}$ . This pole is previously reported in Ref. [34] and is associated with the  $a_1(1260)$  state.

### B. $b_1(1235)$ and $b_1(1400)$

In this subsection, we investigate the existence of possible poles in the solution of Eq. (2), including channels that couple to the quantum numbers  $I^G(J^{PC}) = 1^-(1^{+-})$ , namely  $\pi\omega$ ,  $\phi\pi$ ,  $\rho\eta$ , and  $K^*\bar{K}$ . In Table II, we list the coefficients  $C_{ij}$  corresponding to the possible transitions between those channels, where the  $\omega - \phi$  mixing is considered with mixing angle  $\epsilon_{\omega\phi} = 0.059$  [45].

TABLE II.  $C_{ij}$  coefficients in isospin basis for  $S = 0, I = 1$ .

$b_1$	$\omega\pi$	$\phi\pi$	$\rho\eta$	$K^*\bar{K}$
$\omega\pi$	0	0	0	1
$\phi\pi$	0	0	0	$\epsilon_{\omega\phi}$
$\rho\eta$	0	0	0	$\sqrt{3}$
$K^*\bar{K}$	1	$\epsilon_{\omega\phi}$	$\sqrt{3}$	-1

Note that, from Table II, the WT term for the diagonal transition of the  $K^*\bar{K}$  channel is identical to that in Table I, in Section III. Additionally, this is the only channel with a non-zero diagonal transition. All other channels couple only to  $K^*\bar{K}$ , with the  $\phi\pi$  channel standing out due to the  $\omega - \phi$  mixing. This situation differs from the previous case (see Table I), where Eq. (7) is not fulfilled and the estimation of the coupled channel effect in Eq. (8) still holds, which implies that the interactions from inelastic scattering are perturbative. In the meantime, concerning the  $\phi\pi$  threshold closing to  $b_1(1235)$ , the  $b_1(1235)$  couples to the transitions of  $\phi\pi \rightarrow \phi\pi$  and  $K^*\bar{K} \rightarrow \phi\pi$ , in addition to the WT terms, which causes ambiguity in describing the scattering amplitude in the region around 1200 – 1300 MeV. For the sake of simplicity, the inelastic transitions and the elastic  $\phi\pi$  transition are switched off. Therefore, we can also expect the existence of a pole near  $K^*\bar{K}$  threshold. Indeed, solving Eq. (2) with the coefficients for the WT terms in the single channel scattering, we find virtual poles at  $\sqrt{s_p} = 1331 - i 77$  MeV for  $q_{\max} = 1000$  MeV, and  $\sqrt{s_p} = 1336 - i 130$  MeV if we use  $q_{\max} = 800$  MeV. Similarly to the previous case, in Fig. 7, we depict the modulus square of the diagonal transition amplitude  $K^*\bar{K}$  in the energy range of 1200 MeV to 1600 MeV. Note that the virtual pole manifests itself in the line shape of the

amplitudes in Fig. 7 around 1400 MeV. The corresponding strengths decrease when accounting for the effects of the finite width of the vector mesons, which smooths the curves; however, the bump at 1400 MeV remains visible. It's worth highlighting that calculations from lattice QCD [46] from the HadSpec collaboration suggest an axial-vector state with  $J^{PC} = 1^{+-}$ , analogous to the  $b_1(1235)$ , with a mass and width of 1380 MeV and 91 MeV, respectively. However, the branching ratio of the  $b_1(1235)$  decaying into  $K\bar{K}\pi$  is less than 16 % [40], which implies the  $b_1(1235)$  differs from the molecular  $K^*\bar{K}$ .

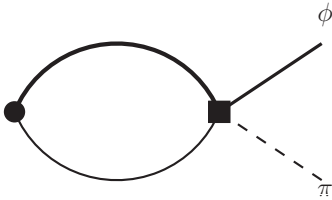


FIG. 6.  $K^*\bar{K}$  transition to  $\phi\pi$  via final state interaction. The black dot and rectangle represent the  $K^*\bar{K}$  production rate and the unitarized scattering amplitude, respectively. The bold, solid and dashed lines stand for the vector mesons, kaon and pion, respectively.

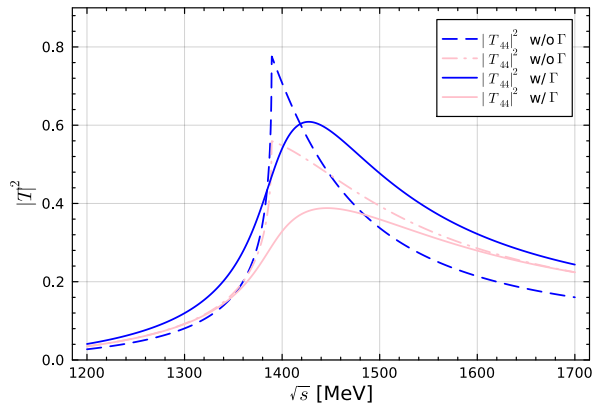


FIG. 7. Modulus squared of  $T$ -matrix elements. The solid and dashed lines correspond to the cases with and without the consideration of the finite width for the vector mesons. The magenta and blue lines are determined by regularizing the loops via dimensional regularization, with the subtractions constant equivalent to a cut-off equal to  $q_{max} = 800$  MeV, and  $q_{max} = 1000$  MeV, respectively.

As this virtual state strongly couples to  $K^*\bar{K}$ , we can search for signals of this state in experimental measurements, which could serve as a test for our model, in the reaction  $J/\psi \rightarrow \eta\phi\pi$  reported by the BESIII collaboration [33]. In particular, in Ref. [33], measurements of the invariant mass distributions  $M_{\pi\eta}$ ,  $M_{\phi\eta}$ , and  $M_{\phi\pi}$  are presented, where, in the latter, a peak is observed at

$M_{\phi\pi} = 1400$  MeV. According to the BESIII collaboration, this signal corresponds to a “non- $\phi$  background”. This signal can also be interpreted as a kinematic effect, that is a TS [32]. However, interpreting this peak as a pure TS is delicate due to Schmid’s Theorem, as discussed by the authors of that work and also pointed out in Ref. [47]. Based on this discussion, we can argue that the peak at 1400 MeV in the  $M_{\phi\pi}$  distribution may, according to our results, be due to the manifestation of the virtual pole discussed above in Fig. 7.

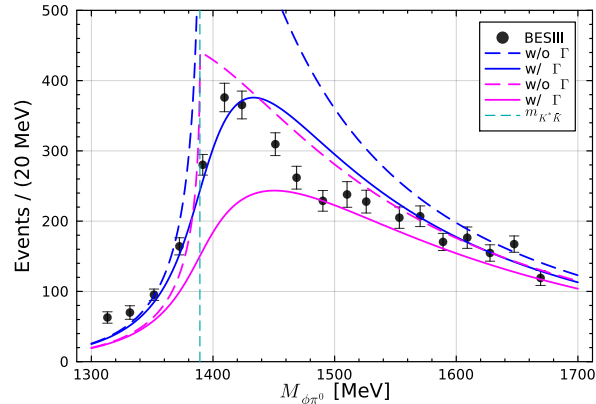


FIG. 8. Numerical results for Eq. (13) compared to the corresponding data from BESIII [33] for the  $\phi\pi$  invariant mass distribution.

To test this hypothesis, we compare our model with the BESIII data. The theoretical expression is given by

$$\frac{dN_{b_1}}{dM_{\text{inv}}} = \frac{1}{8\pi M_{\text{inv}}} |\vec{k}| |\mathcal{M}_{b_1}|^2, \quad (13)$$

where  $N_{b_1}$  represents the number of events, while  $M_{\text{inv}}$  is the invariant mass of the  $\phi\pi$  pair in the final state of the decay  $J/\psi \rightarrow \eta\phi\pi$ . Additionally,  $|\vec{k}|$  denotes the magnitude of the c.m. momentum of the  $\phi\pi$  system. Furthermore,  $\mathcal{M}_{b_1}$  represents the amplitude associated with the diagram in Fig. 6, and given by

$$\begin{aligned} \mathcal{M}_{b_1} &= \tilde{P}_{b_1, K^* \bar{K}} \tilde{G}_{K^* \bar{K}} \tilde{V}_{42} + \tilde{P}_{b_1, K^* \bar{K}} \tilde{G}_{K^* \bar{K}} T_{44} G_{K^* \bar{K}} \tilde{V}_{42} \\ &\simeq P_{b_1, K^* \bar{K}} \tilde{G}_{K^* \bar{K}} T_{44}, \end{aligned} \quad (14)$$

with a constant transition between  $K^* \bar{K}$  and  $\phi\pi$  labelled by  $\tilde{V}_{42}$ , where the pole structure is determined by  $T_{44}$  changes smoothly around  $K^* \bar{K}$  threshold. In Eq. (14),  $P_{b_1, K^* \bar{K}}$  parameterizes the production of the  $K^* \bar{K}$  pair, while  $\tilde{G}_{K^* \bar{K}}$ , similar to the case in Section III, is the  $G$ -loop function of the  $K^* \bar{K}$  pair given by Eq. (3), with its cut-off (or equivalently  $\alpha(\mu)$ ) left as a parameter to be determined through matching with experimental data, along with  $P_{b_1, K^* \bar{K}} \tilde{G}_{K^* \bar{K}}$ .

According to our model, given by Eq. (13), to the BESIII data in Ref. [33] for the  $M_{\phi\pi}$  distribution around 1400 MeV, we obtain the following parameter values:  $P_{b_1, K^*\bar{K}} \approx 122.47 \text{ MeV}^{-1/2}$  and  $q_{\max} = 930 \text{ MeV}$ , the latter corresponding to a subtraction constant of  $\alpha(\mu) = -1.50$ . In Fig. 8, we compare Eq. (13), with those parameters above, to the corresponding data [33]. Overall, we observe a good agreement with the experimental data. In particular, the curves, obtained assuming vector mesons with zero width, describe the data well for values of the  $M_{\phi\pi}$  distribution below the  $K^*\bar{K}$  threshold. In addition, our results, including finite width effects of vector mesons, also match the data perfectly in regions below and above the  $K^*\bar{K}$  threshold, especially above 1500 MeV. On the other hand, in the interval starting from the  $K^*\bar{K}$  threshold ( $\simeq 1387 \text{ MeV}$ ) (dashed blue vertical line) up to around 1450 MeV, although our model does not fit the data perfectly, it can be seen that the line shape of Eq. (13) follows the data trend, peaking at 1410 MeV. It is worth mentioning that, similar to the previous subsection, we employ a very simple model in our comparison in Fig. 8, where the noticeable good agreement with the data seems to indicate that the virtual pole in our results is the dominant contribution to the spectrum in the region where the experimental enhancement at 1400 MeV in Ref. [33] is observed.

In principle, we can assume that the virtual pole in our findings, hereafter denoted as  $b_1(1400)$ , could be assigned to the  $Z_s$  state suggested by the BESIII collaboration [48] as the strange partner of the  $Z_c(3900)$ , observed by BESIII itself in 2013 in the invariant mass distribution  $M_{J/\psi\pi}$  in the decay  $Y(4260) \rightarrow J/\psi\pi^+\pi^-$ . Specifically, in Ref. [48], the BESIII collaboration sought evidence of the  $Z_s$  state in the invariant mass distribution of the  $\phi\pi$  pair, based on data from the reaction  $e^+e^- \rightarrow \phi\pi\pi$ . However, no signal of that state is found. This result is further supported by lattice results in Ref. [46], where the authors stated that they do not find any signal of the  $Z_s$  state in  $\phi\pi$  channel. As we know, this reaction produces states with  $J^{PC} = 1^{--}$ , and since many channels couple to this set of quantum numbers, they can decay into  $\phi\pi\pi$ , where interference effects among these various channels may smear the  $Z_s$  signal in the  $\phi\pi$  channel. On the other hand, the isospin-violating process  $J/\psi \rightarrow \eta\phi\pi$  could be a good option since it is free from such interference, thus potentially revealing a signal, if it exists, of the  $Z_s$  state, which would be an essentially exotic strangeonium-like state.

#### IV. ISOSCALAR SPECTRUM

In this section, we explore the isoscalar sector. That is, we will search for states dynamically generated by  $PV$  interactions with channels coupling to quantum numbers  $I^G(J^{PC}) = 0^\pm(1^{+\pm})$ .

Next, we will begin our discussion with the positive  $G$ -parity sector.

### A. $f_1(1285)$ and $f_1(1420)$

In this case, in the region of interest, namely around the  $K^*\bar{K}$  mass threshold, we have a single channel, which is the  $K^*\bar{K}$  itself, with the WT term given in Table III. Here, we adopt a different strategy from previous cases. Specifically, we use experimental data from the OBELIX collaboration [49] to adjust our model by fixing the cutoff  $q_{\max}$  (or equivalently the subtraction constant) so that our theoretical curve matches the data for the  $K^*\bar{K}$  mass distribution. Once the cutoff is fixed, we search for poles in the solution of Eq. (2), in order to investigate if the  $K^*\bar{K}$  interaction leads to the dynamical generation of any state.

TABLE III.  $C_{ij}$  coefficients in isospin basis for  $S = 0, I = 0$ .

$f_1$	$K^*\bar{K}$
$K^*\bar{K}$	-3

Experimentally, in this sector, there are two structures, namely  $f_1(1285)$  and  $f_1(1420)$ , which in principle can couple to the  $K^*\bar{K}$  channel, given that both have been measured in various experiments in  $K^*\bar{K}$  ( $K^* \rightarrow K\pi$ ) as the final product of the studied reactions. In particular, the  $f_1(1285)$  structure is considered, which is one of the two isosinglets  $f_1$  states of the low-lying axial-vector meson  $1^{++}$  nonet. However, according to previous studies [34, 50], this structure can also be interpreted as a  $K^*\bar{K}$  molecular state. On the other hand, the  $f_1(1420)$  structure, first observed in the process  $\pi^- p \rightarrow K_S^0 K^\pm \pi^\mp \eta$ , despite being listed in the RPP as a resonance with  $0^+(1^{++})$ , its interpretation is highly debated. For instance, in Refs. [51, 52] the authors pointed out that the  $f_1(1420)$  is an effect stemming from the  $K^*\bar{K}$ .

Moreover, in the quark model, the axial-vector mesons  $f_1(1285)$  and  $f_1(1420)$  are members of the  $1^3P_1$  states. In particular, they are considered to be mixtures of the pure octet and singlet, denoted as  $f_8$  and  $f_1$ , respectively, with  $\theta$  parameterizing the mixing angle. In Ref. [53], the LHCb collaboration measured  $\theta$  from the ratio of decay rates of  $\bar{B}^0 \rightarrow J/\psi f_1(1285)$  and  $\bar{B}_s^0 \rightarrow J/\psi f_1(1285)$ , concluding that the measurement is consistent with other studies in which the  $f_1(1285)$  structure mixes with  $f_1(1420)$ . Furthermore, the value of this ratio estimated by the tetraquark model for  $f_1(1285)$  in Ref. [54] is at 3.3 standard deviations from the value obtained by the measurement reported by LHCb [53].

We can take into account the effects of a possible  $q\bar{q}$  configuration for both structures above in our model. This type of mixture is widely studied in hadron physics [55–62]. Assuming that the  $K^*\bar{K}$  channel couples to both isosinglets  $f_1(1285)$  and  $f_1(1420)$ , we can describe such couplings using the following effective interactions,

$$\begin{aligned}\mathcal{L}_1 &= g_1 \bar{K} K^{*,\mu} f_{1,\mu}^1, \\ \mathcal{L}_8 &= g_8 \bar{K} K^{*,\mu} f_{1,\mu}^8,\end{aligned}\tag{15}$$

where  $g_1$  and  $g_8$  define the couplings of the  $K^*\bar{K}$  channel to the bare states members of the singlet  $f_1^1$  and the pure flavor octet  $f_1^8$ , respectively, while the masses of  $f_1^1$  and  $f_1^8$  are  $m_1$  and  $m_8$ , respectively.

In the S-wave, the interactions in Eq. (15) introduce a correction to the WT term, describing the amplitude of  $K^*\bar{K} \rightarrow K^*\bar{K}$ , given by

$$\begin{aligned}\tilde{V} &= V_{WT} + \frac{g_1^2}{s - m_1^2 + i m_1 \Gamma_1} + \frac{g_8^2}{s - m_8^2 + i m_8 \Gamma_8}, \\ &= V_{WT} + \frac{(g_1^2 + g_8^2)(s - \tilde{m}^2)}{\left[s - \frac{1}{2}(\tilde{m}_1^2 + \tilde{m}_8^2)\right]^2 - \frac{1}{4}(\tilde{m}_1^2 - \tilde{m}_8^2)^2}, \\ &= V_{WT} + \delta V,\end{aligned}\tag{16}$$

with  $\tilde{m}^2 = (g_1^2 \tilde{m}_8^2 - g_8^2 \tilde{m}_1^2) / (g_1^2 + g_8^2)$  and  $\tilde{m}_{1(8)}^2 = m_{1(8)}^2 - i m_{1(8)}^2 \Gamma_{1(8)}$ , where the  $\Gamma_{1(8)}$  corresponds to the contribution from lower channels that leads complex  $[q\bar{q}]$  poles in the energy plane. Concerning  $\Gamma_{1(8)}$  is narrow, and the  $\delta V$  is perturbative,

$$\tilde{T}^{-1} = \frac{1}{V_{WT}} - \tilde{G}_{K^*\bar{K}},\tag{17}$$

where  $\tilde{G}_{K^*\bar{K}} = \delta V / V_{WT}^2 + G_{K^*\bar{K}}$ . That is, the term  $\delta V / V_{WT}^2$  can be absorbed into the subtraction constant  $\alpha(\mu)$  in the loop function  $G_{K^*\bar{K}}$ . In other words, the  $q\bar{q}$  contribution corresponding to the second term in Eq. (16) in our model has the effect of modifying the subtraction constant in Eq. (4), which will be determined by adjusting the  $K^*\bar{K}$  invariant mass to the corresponding data from OBELIX [49].

Next, we discuss the invariant mass distribution of the  $K^*\bar{K}$  pair. The  $f_1(1420)$  structure exclusively decays via  $K^*\bar{K}$ , giving us

$$\Gamma_{f_1} = |\mathcal{M}_{f_1}|^2 \frac{|\vec{p}_{K^*}|}{8\pi M_{K^*\bar{K}}},\tag{18}$$

where  $|\vec{p}_{K^*}|$  represents the magnitude of the momentum of the outgoing  $K^*$  meson in the c.m. frame of the  $K^*\bar{K}$  pair with total energy  $M_{K^*\bar{K}}$ . Moreover,  $\mathcal{M}_{f_1}$  is the production amplitude

given by

$$\mathcal{M}_{f_1} = P_{K^*\bar{K}}^{f_1} G_{K^*\bar{K}} \tilde{T}_{f_1}, \quad (19)$$

with  $P_{K^*\bar{K}}^{f_1}$  parametrizing the production rate of the  $K^*\bar{K}$  pair. The distribution of interest is obtained by multiplying Eq. (18) by the  $K^*$  meson spectral function [63–65], taking into account the decay  $K^* \rightarrow K\pi$ . Therefore, we have

$$\frac{dN_{f_1}}{dM_{[K\pi]\bar{K}}} = \frac{1}{\mathcal{N}} \int_{m_K+m_\pi}^{M_{[K\pi]\bar{K}}-m_{\bar{K}}} dE_{K^*} \Gamma(M_{[K\pi]\bar{K}}, E_{K^*}) \rho^{K\pi}, \quad (20)$$

with a norm factor  $\mathcal{N}$ <sup>1</sup>, where  $\rho^{K\pi}$  is the  $K^*$  spectral function

$$\rho^{K\pi} = -\frac{2M_{K^*}}{\pi} \text{Im} \frac{1}{E_{K^*}^2 - M_{K^*}^2 + iM_{K^*}\Gamma_{K^*}(E_{K^*})}, \quad (21)$$

with

$$\Gamma_{K^*}(E_{K^*}) = \Gamma_{K^*} \left( \frac{p^{\text{off}}}{p^{\text{on}}} \right)^3, \quad (22)$$

$$p^{\text{off}} = \frac{\lambda^{1/2}(E_{K^*}^2, m_\pi^2, m_K^2)}{2E_{K^*}} \theta(E_{K^*} - m_\pi - m_K), \quad (23)$$

$$p^{\text{on}} = \frac{\lambda^{1/2}(M_{K^*}^2, m_\pi^2, m_K^2)}{2M_{K^*}}, \quad (24)$$

$$\lambda(x, y, z) = x^2 + y^2 + z^2 - 2xy - 2yz - 2zx. \quad (25)$$

$M_{[K\pi]\bar{K}}$  is equivalent to the  $M_{K^*\bar{K}}$ .  $\Gamma_{K^*} = 50$  MeV is an averaged  $K^*$  width.

In Fig. 9, we present the comparison between the distribution according to Eq. (20) and the data from the OBELIX collaboration [49]. From this comparison, we can achieve a good agreement with the data by adjusting  $P_{K^*\bar{K}}^{f_1} = 63.25$  MeV<sup>-1/2</sup> and  $\alpha(\mu) = -0.4$  in the T-matrix. Remarkably, the dashed line represents the distribution in which the transition amplitude, given by Eq. (20), does not account for the width of the  $K^*$  meson. We observe a prominent peak around 1400 MeV, corresponding to the manifestation of a virtual pole at 1385 MeV at the second Riemann sheet below the  $K^*\bar{K}$  threshold, derived from the solution of Eq. (20), with the value of the subtraction constant determined above. On the other hand, including the width of the  $K^*$  meson in Eq. (17) affects the distribution (solid curve), reducing its strength across the entire range of  $M_{K^*\bar{K}}$ , especially in the vicinity of 1400 MeV. This results in a better agreement with the data in the low-energy part of the distribution, as well as in the region above 1450 MeV. Initially, we cannot draw many conclusions from this comparison, as it is somewhat hindered by the scarcity of data in the region of interest.

<sup>1</sup> This factor is absorbed into the redefined production rate.

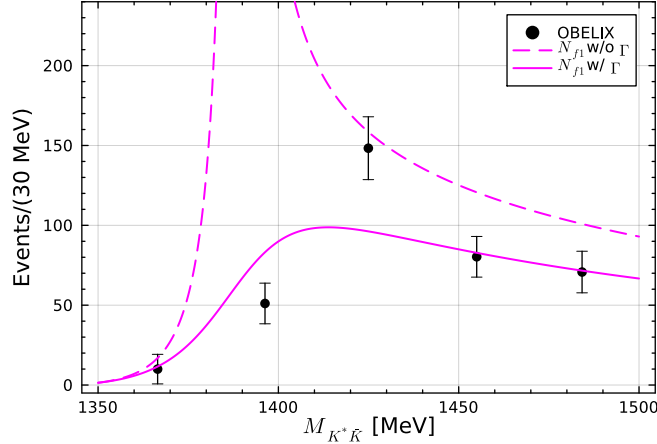


FIG. 9. Comparison between the theoretical invariant mass distribution, as given by Eq. (20), and the corresponding experimental data from OBELIX [49].

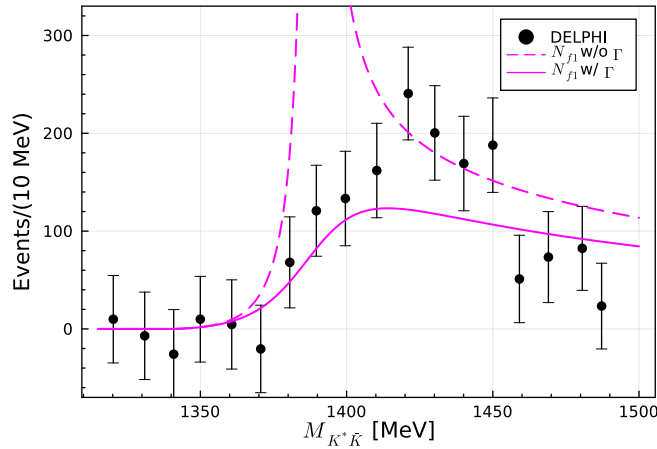


FIG. 10. Comparison between numerical results for Eq. (20) associated with the  $K^*\bar{K}$  invariant mass distribution and the corresponding data from DELPHI experiment [66].

Figure 10 illustrates a new comparison between Eq. (20) and the corresponding distribution released by the DELPHI collaboration [66], which features a more comprehensive dataset than OBELIX. Similar to Fig. 9, we achieve an excellent agreement with the data from Ref. [66] in both low and high-energy regions of the spectrum. We particularly highlight the region around 1400 MeV, where the curve, including the width of the  $K^*$  meson, fits perfectly with the dataset in this range.

In principle, within the uncertainties of our model, we could relate the virtual state in our results to the nontrivial  $f_1(1420)$  structure presented in the data from the OBELIX [49] and DELPHI [66] collaborations. However, asserting categorically that the  $f_1(1420)$  structure is a virtual state would

be premature, given the simplicity of our model. On the other hand, what we can confidently state is that the nontrivial structure around 1400 MeV in the data from Refs. [49, 66] is well described in our model as a result of a dynamically generated state from the  $K^*\bar{K}$  interaction, which does not conflict with the conclusion in Ref. [51]. Consequently, if the behavior of the data in this region is attributed to the  $f_1(1420)$  structure, we can conclude that such a structure possesses a sizable  $K^*\bar{K}$  component, according to our findings. This is similar to the *small-binding* molecule mixing with a bare state, where the nature of the hadron can be unveiled by extracting the scattering length and effective range [67, 68]

The  $f_1(1285)$  is reported in  $\gamma p \rightarrow \eta\pi^+\pi^-p$  in Ref. [69], where the  $f_1(1285)$  decays into  $\eta\pi^+\pi^-$ , and the signal for the  $f_1(1420)$  is not confirmed. This implies that the production rates of  $f_1(1285)$  and  $f_1(1420)$  are different. This difference in production also appears in  $J/\psi \rightarrow \phi\eta\pi^+\pi^-$  [70], where only the  $f_1(1285)$  is mentioned. Moreover, the  $f_1(1285)$  decays into  $4\pi$  with a branching fraction of  $32.7 \pm 1.9\%$  [71], where the  $4\pi$  weakly couple to the isoscalar  $K^*\bar{K}$  scattering. Therefore, a sizable component of the  $f_1(1285)$  might not be a  $K^*\bar{K}$  molecule, which is plausible given the large mass difference between the  $f_1(1285)$  and the  $K^*\bar{K}$  threshold. It is natural to conclude that the  $f_1(1285)$  has a sizable non-molecular component, such as a  ${}^3P_1 [q\bar{q}]$  state in the quark model [40].

### B. $h_1(1170)$ and $h_1(1415)$

In  $G = -1$ ,  $I = 0$  sector,  $h_1(1170)$  and  $h_1(1415)$  are on the RPP, and attributed to be the  ${}^1P_1 [q\bar{q}]$ , which can also couple to the VP channels, where the interference between  $[q\bar{q}]$  and the WT terms is absorbed by the subtractions in the loops. In Table IV, we list the  $C_{ij}$  coefficients of the WT terms describing the transitions, among the following channels:  $\rho\pi$ ,  $\omega\eta$ ,  $K^*\bar{K}$ , and  $\phi\eta$ .

TABLE IV.  $C_{ij}$  coefficients in isospin basis for  $S = 0, I = 0$ .

$h_1$	$\rho\pi$	$\omega\eta$	$K^*\bar{K}$	$\phi\eta$
$\rho\pi$	-4	0	$\sqrt{3}$	0
$\omega\eta$	0	0	$-\sqrt{3}$	0
$K^*\bar{K}$	$\sqrt{3}$	$-\sqrt{3}$	-3	$\sqrt{6}$
$\phi\eta$	0	0	$\sqrt{6}$	0

In this case, the only non-zero diagonal transitions are those for the  $\rho\pi$  and  $K^*\bar{K}$  channels. Additionally, note that all non-zero off-diagonal transitions involve the  $K^*\bar{K}$  channel. In particular,

comparing the  $C_{ij}$  for the diagonal transitions  $\rho\pi$  and  $K^*\bar{K}$  with their counterparts for the  $G = +1$ ,  $I = 1$  sector, as shown in Table I, we notice that in the current case, the coefficients are larger, doubling for the  $\rho\pi$  channel and tripling for the  $K^*\bar{K}$  channel. Thus, we can anticipate the existence of poles in the solution of Eq. (2), with the coefficients  $C_{ij}$  in Eq. (1), given in Table IV. Indeed, we obtain two poles: one at  $931_{-12}^{+12} - i35_{-16}^{+23}$  MeV, strongly coupled to the  $\rho\pi$  channel, and another at  $1296_{-49}^{+42} - i7_{-1}^{+7}$  MeV, coupling to the  $K^*\bar{K}$  channel, with the uncertainties in both cases due to variations of about 200 MeV in the cutoff  $q_{max} = 800$  MeV, while the poles are  $931_{-11}^{+11} - i36_{-15}^{+22}$  MeV and  $1327_{-41}^{+38}$  MeV with switching off the inelastic transitions and may relate to the  $h_1$ 's below 1400 MeV in Ref. [72]. In Ref. [34], a pole at  $919 - i17$  MeV is also reported in the  $G = -1$  sector in the  $\rho\pi$  channel, identified by the authors with the resonance  $h_1(1170)$ . According to RPP [40], the corresponding experimental mass value of  $h_1(1170)$  state is  $1166 \pm 6$  MeV, with a large width around  $375 \pm 35$  MeV.

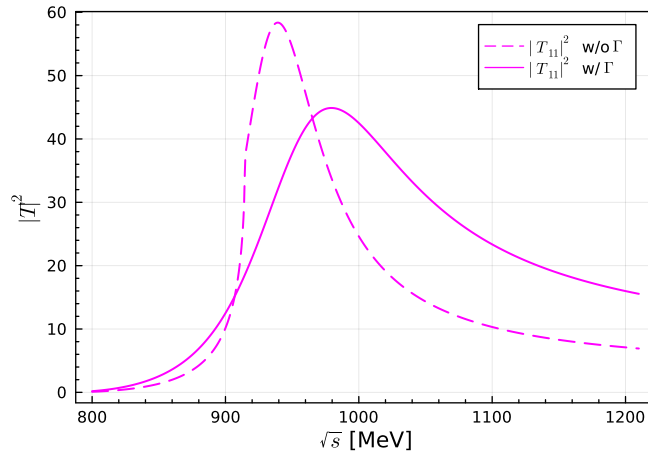


FIG. 11. Modulus squared of the  $T$ -matrix element with  $\alpha(\mu)$  equivalent to a cut-off choice of about  $q_{max} = 800$  MeV.

In Fig. 11, we show the modulus squared of the  $\rho\pi \rightarrow \rho\pi$  transition, where, similar to previous cases, we also take into account the non-zero width of vector mesons. Note that the pole at 933 MeV manifests around 940 MeV. Including the non-zero width, the peak shifts by 50 MeV, around 980 MeV, with a slight decrease in strength.

On the other hand, the higher pole could be responsible for the peak near 1415 MeV in the invariant mass distribution of the  $K^*(892)\bar{K}$  pair in the  $\chi_{cJ} \rightarrow \phi K^*\bar{K}$  reaction, as measured by BESIII [73]. According to Ref. [73], this signal at 1415 MeV is assigned to the  $h_1(1380)$  resonance, recently renamed by the RPP as  $h_1(1415)$ , previously measured by the LASS [74] and Crystal Barrel [75] collaborations. We can study the impact of the higher pole on the invariant mass

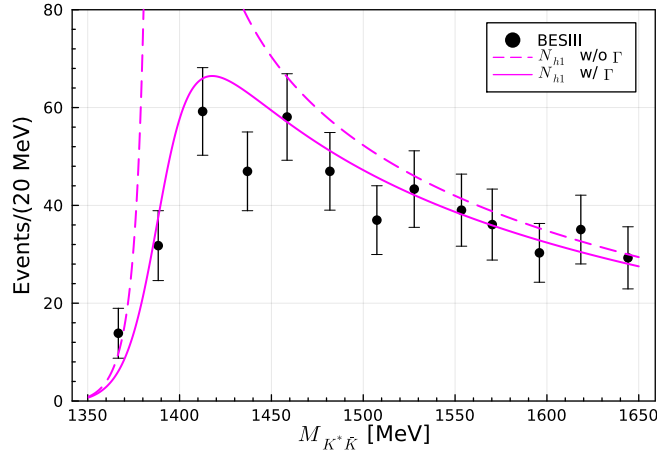


FIG. 12. Numerical results for the invariant mass distribution, given in Eq. (26), compared to the corresponding data from BESIII collaboration [73]. The  $K^*\bar{K}$  loops are regularized with  $\alpha(\mu) = -0.4$ , corresponding to  $q_{max} = 385$  MeV in the cut-off regularization scheme, while  $P_{K^*\bar{K}}^{h_1} = 47.43 \text{ MeV}^{-1/2}$ .

distribution measured by BESIII in Ref. [73], in an attempt to interpret this pole possibly as the  $h_1(1415)$  state of the RPP [71], using the equations already discussed in the previous subsection, with parameters suitable for the present case. Thus, we have

$$\frac{dN_{h_1}}{dM_{[K\pi]\bar{K}}} = \frac{1}{\mathcal{N}_{h_1}} \int_{m_K+m_\pi}^{M_{[K\pi]\bar{K}}-m_{\bar{K}}} dE_{K^*} \Gamma_{h_1}(M_{[K\pi]\bar{K}}, E_{K^*}) \rho^{K\pi}, \quad (26)$$

with

$$\Gamma_{h_1}(M_{K^*\bar{K}}, E_{K^*}) = |\mathcal{M}_{h_1}|^2 \frac{|\vec{k}_{K^*}|}{8\pi M_{K^*\bar{K}}}, \quad (27)$$

and

$$\mathcal{M}_{h_1} = P_{K^*\bar{K}}^{h_1} \tilde{G}_{K^*\bar{K}}^{h_1} T_{h_1}. \quad (28)$$

The  $\mathcal{N}_{h_1}$  is a norm factor, which is absorbed into the production rate  $P_{K^*\bar{K}}^{h_1}$ .  $\tilde{G}_{K^*}^{h_1}$  and  $T_{h_1}$  are the  $K^*\bar{K}$  loop function and the unitarized scattering amplitude in elastic  $K^*\bar{K}$  scattering.

In Fig. 12, we show the comparison between Eq. (26) and the experimental data from Ref. [73]. The dashed line represents the distribution obtained when we do not consider the effects of the finite width of vector mesons. Despite the clear disagreement between our results and the experiment, a sharp peak shows up around 1415 MeV, exactly in the region where the experimental peak associated with the  $h_1(1415)$  state is observed. On the other hand, our theoretical curve fits well with the data in the regions below 1400 MeV and above 1450 MeV. The comparison is improved in the whole range when we take into account the effects of the finite width of vector mesons, as

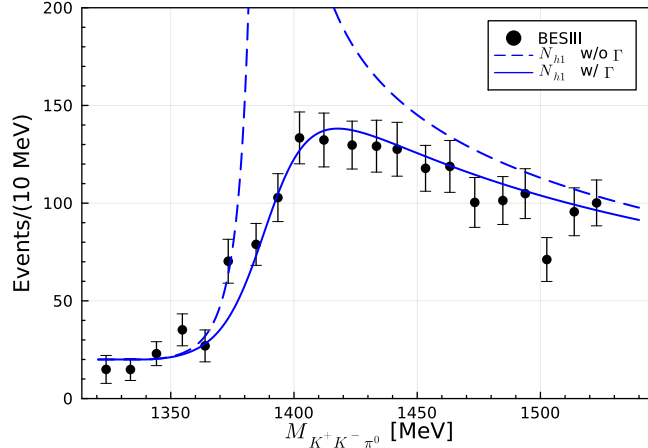


FIG. 13. Comparison between the theoretical  $K\bar{K}\pi$  mass spectrum, as given in Eq. (26), and the recent data from BESIII [76], obtained for  $P_{K^*\bar{K}}^{h_1} = 63.25 \text{ MeV}^{-1/2}$ ,  $q_{max} = 385 \text{ MeV}$ , and  $c_1 = 0.005 \text{ MeV}^{-1}$ .

can be seen in Fig. 12, where the solid curve fits the data very well, including the peak region at 1415 MeV.

At first glance, we are led to believe that the higher pole manifesting in the region of the  $h_1(1415)$  resonance could explain the data from BESIII [73]. Consequently, we might conclude that the resonance could be understood as a dynamically generated state by the coupled-channel interaction of  $K^*\bar{K}$ , as described in Table IV. However, the good agreement between our results and the data in Fig. 12 should be interpreted with care since it is obtained for low values of  $q_{max}$  (approximately 385 MeV).

On the other hand, there is new data on  $h_1(1415)$  in  $K\bar{K}\pi$  invariant mass distribution from BESIII [76]. This can be understood by introducing a constant background term  $c_1$  to Eq. (26),

$$\frac{d\tilde{N}_{h_1}}{dM_{[K\pi]\bar{K}}} = \frac{dN_{h_1}}{dM_{[K\pi]\bar{K}}} + c_1, \quad (29)$$

where the background term  $c_1$  indicates the final state interaction from  $K\bar{K}\pi$  and the ratio in the phase spaces between  $K^*\bar{K}$  and  $K\bar{K}\pi$  is parametrized into the production rate.

In Fig. 13, we show the numerical results corresponding to Eq. (29). Specifically, we make a comparison to the  $K\bar{K}\pi$  invariant mass distribution, recently reported by BESIII experiment [76], from  $J/\psi \rightarrow \eta' K\bar{K}\pi$  decay. We note that our results match well the data within the range considered for the constant background term  $c_1$  equals to  $0.005 \text{ MeV}^{-1}$ , while  $q_{max}$  is fixed with the same value as in Fig. 12, with a slightly change in the  $P_{K^*\bar{K}}^{h_1}$  parameter. In particular, the higher pole at 1372 MeV dominates the distribution around 1415 MeV, exactly where the  $h_1(1415)$  resonance manifests in the data, with an even better agreement when the  $K^*$  meson width is taken

into account in our description.

## V. STRANGE SPECTRUM

### A. $K_1(1270)$

In what follows, we discuss the  $K_1(1270)$  state, which is described as a mixture of flavor eigenstates  $K_{1A}$  and  $K_{1B}$  in the quark model. However, according to the ChU approach, this state is actually associated with a double-pole structure resulting from  $PV$  interaction in the  $I(J^P) = 1/2(1^+)$  sector [77, 78]. In Ref. [77], the authors studied this interaction considering coupled channels within the range of 1032 MeV to 1500 MeV. In Table V, we list the relevant channels considered in Ref. [77] along with the  $C_{ij}$  coefficients of the WT terms describing the interactions between these channels. According to the results of Ref. [77], two poles are obtained: one at  $1195 - i 123$  MeV, strongly coupled to the  $K^*\pi$  channel, and a higher one at  $1284 - i 73$  MeV, coupling more to the  $\rho K$  channel, which is supported by the recent study of correlation function [79].

Based on the results in Table V, we search for virtual poles in the solutions of Eq. (2). However, no virtual state is found. On the other hand, we obtained, as expected, a double-pole structure on  $RS_{-++++}$ : one at  $1126_{-17}^{+15} - i 91_{-26}^{+39}$  MeV and another at  $1250_{-32}^{+18} - i 3_{-3}^{+1}$  MeV with a small imaginary part due to the weak coupling with the  $K^*\pi$  channel, which is open. For the case of switching of the inelastic transitions, the poles are  $1131_{-8}^{+5} - i 117_{-23}^{+30}$  MeV and  $1261_{-19}^{+6}$  MeV. At this point, it is important to emphasize that, at first glance, our approach seems identical to that of Ref. [77]. However, they differ in how we incorporate the effects of the finite width of vector mesons. In Ref. [77], such effects are taken into account by convoluting the loop function with the spectral function of the vector meson, which is related to the propagator through the Källén-Lehmann representation. However, this approach alters the analytical structure of the loop function and consequently affects the interpretation of the poles in the solution of Eq. (2) as bound states/resonances or virtual states. Therefore, in our case, we consider the finite width of the vector mesons involved in the loop by using a complex mass  $M \rightarrow M - i\Gamma/2$ , where  $\Gamma$  is the width of the vector meson.

This approach also changes the analytical structure of the  $G$ -loop function, but now we can no longer claim any interpretation of the poles as bound states/resonances or virtual states, and therefore, we only focus on the impact of these structures on the line shape of the amplitudes of interest, as shown in Fig. 14. In it, we can see a dip at 1262 MeV, which disappears when we

TABLE V.  $C_{ij}$  coefficients in isospin basis for  $S = 1, I = \frac{1}{2}$  [34].

$K_1$	$K^*\pi$	$\rho K$	$\omega K$	$K^*\eta$	$\phi K$
$K^*\pi$	-2	$\frac{1}{2}$	$\frac{\sqrt{3}}{2}$	0	$-\sqrt{\frac{3}{2}}$
$\rho K$	$\frac{1}{2}$	-2	0	$-\frac{3}{2}$	0
$\omega K$	$\frac{\sqrt{3}}{2}$	0	0	$\frac{\sqrt{3}}{2}$	0
$K^*\eta$	0	$-\frac{3}{2}$	$\frac{\sqrt{3}}{2}$	0	$-\sqrt{\frac{3}{2}}$
$\phi K$	$-\sqrt{\frac{3}{2}}$	0	0	$-\sqrt{\frac{3}{2}}$	0

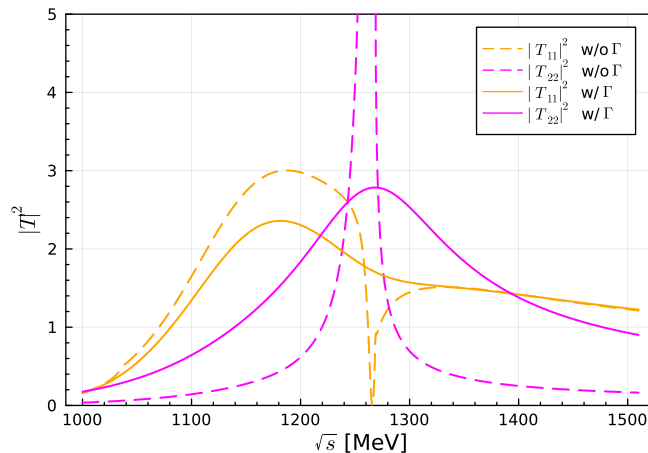


FIG. 14. Modulus squared of the  $T$ -matrix element for the value of the subtraction constant  $\alpha(\mu)$  obtained by matching the cut-off scheme at threshold for  $q_{max} = 800$  MeV. The subscript  $i = 1, 2$  corresponds to the channels  $K^*\pi$  and  $\rho K$ , respectively.

include the widths of the vector mesons, resulting in a smooth curve with a broad bump in the region of the lower pole. Interestingly, despite the dip manifesting in the line shape for the  $K^*\pi$  channel, where the lower pole shows up, it is located exactly in the region where the higher pole dominates. This effect highlights the influence of the coupled channel on the system in question.

In addition to the dynamically generated poles in  $K_1(1270)$  spectrum, the  $^3P_1$  and  $^1P_1$  states mix and couple to the  $VP$  scattering, where the interference between configurations is similar to the one  $a_1(1260)$  spectrum. The line shapes in Fig. 14 are probably revised. The deformation on the line shapes provides hints for probing the interference. Besides the  $K_1(1270)$ , a broad  $K_1(1400)$  is included in the RPP [40]. Its mass closes to  $K^*\eta$  threshold. There is no block to have a transition between  $[q\bar{q}]$  and  $VP$  channel, which deserves further studies.

## B. Isoscalar $K^*K$ scattering

At this point, it is worth briefly commenting on the  $K^*K$  interaction. If such an interaction is strong enough to produce a pole in the solution of the unitarized transition amplitude for the  $K^*K$  single-channel case, that pole could potentially be associated with a  $T_{ss}$  hadronic state with  $\bar{s}\bar{s}ud$  quark content, which is the flavor-partner of the  $T_{cc}$  state, a  $DD^*$  molecular structure [80–88]. In terms of  $K^*$  and  $K$ , the  $|\bar{s}\bar{s}ud\rangle$  tetraquark wave function for  $I = 0$  is written as

$$|\bar{s}\bar{s}ud\rangle = \frac{1}{\sqrt{2}}|K^{*+}K^0\rangle - \frac{1}{\sqrt{2}}|K^{*0}K^+\rangle. \quad (30)$$

From that, we have evaluated the corresponding WT term describing the  $K^*K$  transition, which vanishes, indicating that if such an interaction produces the  $T_{ss}$ , it should occur through another mechanism. On the other hand, we can consider that the  $K^*K$  interaction takes place through  $a_1(1420)$  exchange, similar to the  $a_1(1260)$  exchange in the  $Z_c$  spectrum [89]. According to our discussion on the isovector sector in Section III, by assuming  $a_1$  as the virtual state stemming from the  $K^*\bar{K}$  interaction, we can easily determine the  $a_1$  coupling to the  $K^*\bar{K}$  channel,  $g_{a_1}$ , from which we can evaluate the  $K^*K \rightarrow K^*K$  transition. We have determined that

$$V^{a_1} \simeq \mathcal{O}\left(\frac{g_{a_1}^2}{m_{a_1}^2}\right), \quad (31)$$

with  $g_{a_1}$  of the order of  $\mathcal{O}(5 \text{ GeV})$ . By comparing the strength at threshold with the  $K^*\bar{K}$  interaction, we note that  $|V^{a_1}| \sim |V_{K^*\bar{K}}^{I=1}|/10$ , which is ten times smaller than the  $K^*\bar{K}$  interaction and weaker than the  $K^*K$  interactions in the quark model [90, 91] and one-boson exchange model [92, 93]. Such an interaction is too weak to dynamically generate a pole near the  $K^*K$  threshold. The existence of the  $T_{ss}$  is still an open question and deserves further study, both theoretically and experimentally.

## VI. SUMMARY

Using the ChU approach, we explore the interactions between pseudoscalar and vector mesons to investigate the axial-vector structures in the positive and negative G-parity sectors within the energy range around the  $K^*\bar{K}$  mass threshold. Specifically for the isovector sector with  $G = +1$ , from the  $K^*\bar{K}$  interaction, we find a pole on the second Riemann sheet below the threshold, corresponding to a virtual state. We show that this state is likely responsible for the nontrivial structure around 1400 MeV observed in the invariant mass spectrum of the  $f_0(980)\pi^0$  pair reported by the COMPASS collaboration, previously identified as a genuine resonance called  $a_1(1420)$ . However,

some studies suggested that this structure is actually a kinematic effect resulting from the decay of the  $a_1(1260)$  resonance into the  $K^*\bar{K}$  pair, where the  $K^*$  meson subsequently decays into  $K\pi$ , causing a loop formed by the intermediate states  $K^*$ ,  $\bar{K}$ , and  $K$  to give rise to a singularity when these mesons are on the mass shell. In contrast, our results support an interpretation where the  $a_1(1420)$  is a virtual state generated by the  $K^*\bar{K}$  interaction. Additionally, when we perturbatively include the  $\rho\pi$  channel, no significant changes are observed in our analysis. However, we find a second pole at 1120 MeV in the unitarized scattering amplitude solution with two channels,  $K^*\bar{K}$  and  $\rho\pi$ , in the diagonal transition  $\rho\pi \rightarrow \rho\pi$ . This pole is 80 MeV below the central value of the  $a_1(1260)$  experimental mass. This could suggest a significant  $q\bar{q}$  component in the wave function of this structure.

On the other hand, our investigation in the  $G = +1$  sector reveals a virtual state that strongly couples to the  $K^*\bar{K}$  channel. This virtual state appears in the  $\phi\pi$  mass spectrum measured by the BESIII experiment in the  $J/\psi \rightarrow \eta\phi\pi$  decay. Some interpretations attribute this signal to a TS effect. However, it is not purely a TS due to interference with the tree-level contribution, which, according to Schmid's theorem, plays an important role in that decay process. Conversely, we found no pole that could be assigned to the broad structure  $b_1(1235)$ . In particular, due to its broadness, it overlaps with the  $\phi\pi$  and  $\rho\eta$  mass thresholds. However, within our approach, no significant dynamics arise from these coupled channels because the corresponding WT terms among these channels vanish.

As for the isoscalar sectors, we have shown that the  $q\bar{q}$  contribution to the PV interactions in the  $G = +1$  case can be absorbed by the subtraction constant  $\alpha(\mu)$  used to regulate the PV loops. Because of this, we adopt a strategy that fixes the values of  $\alpha(\mu)$  by comparing them to the available data. As a result, we obtain a pole that dominates the corresponding mass spectra reported by the OBELIX and BESIII experiments around 1400 MeV, precisely in the mass region where the  $f_1(1420)$  resonance appears. Therefore, if the nontrivial line shape around 1420 MeV present in both datasets is solely due to the  $f_1(1420)$ , we can state that it has a sizable  $K^*\bar{K}$  component, as the pole in our findings appears in the spectra under consideration due to its strong coupling to the  $K^*\bar{K}$  channel. As for the  $f_1(1285)$ , although some works suggest it is a deeply bound  $K^*\bar{K}$  state, within the procedure we adopt, the nature of this meson might be an admixture of  $K^*\bar{K}$  and  $[q\bar{q}]$ .

Finally, for the  $G = -1$  case, we also obtain two poles due to the similarity with the  $\rho\pi$  and  $K^*\bar{K}$  coupled-channel case, as shown by the WT terms. The lower pole couples to the  $\rho\pi$  channel, while the higher pole primarily couples to  $K^*\bar{K}$ . The former pole can be identified with

the  $h_1(1170)$  resonance listed in the RPP. On the other hand, we have shown that the latter pole is likely responsible for the peak observed near 1415 MeV in the  $K^*\bar{K}$  mass spectrum from the  $\chi_{cJ} \rightarrow \phi K^*\bar{K}$  decay reported by the BESIII collaboration, which is identified as the  $h_1(1415)$ .

The axial-vector meson spectrum, involving the mixture of  $[q\bar{q}]$  and molecule, provides a good situation to unveil the strong interaction in the non-perturbative regime. We suggest searching  $a_1(1420)$  and  $b_1(1400)$  in  $\rho\pi$  and  $\omega\pi$  invariant mass distributions, respectively. In particular, the  $b_1(1400)$  is a flavor partner of  $Z_c(3900)$ .

### ACKNOWLEDGMENTS

We would like to thank Prof. Feng-Kun Guo for his suggestion on this study and Dr. J. M. Dias for his contributions at the early stage of this project. We also thank Profs. E. Oset, Wei-Hong Liang, and Chu-Wen Xiao for their valuable discussions. This research is supported by the National Natural Science Foundation of China under Grants No. 12305096, the Fundamental Research Funds for the Central Universities under Grant No. SWU-XDJH202304, No. SWU-KQ25016 and Chongqing Natural Science Foundation under Project No. CSTB2025NSCQ-GPX0516.

- 
- [1] H.-X. Chen, W. Chen, X. Liu, and S.-L. Zhu, *Phys. Rept.* **639**, 1 (2016), [arXiv:1601.02092 \[hep-ph\]](#).
  - [2] A. Hosaka, T. Iijima, K. Miyabayashi, Y. Sakai, and S. Yasui, *PTEP* **2016**, 062C01 (2016), [arXiv:1603.09229 \[hep-ph\]](#).
  - [3] A. Esposito, A. Pilloni, and A. D. Polosa, *Phys. Rept.* **668**, 1 (2017), [arXiv:1611.07920 \[hep-ph\]](#).
  - [4] R. F. Lebed, R. E. Mitchell, and E. S. Swanson, *Prog. Part. Nucl. Phys.* **93**, 143 (2017), [arXiv:1610.04528 \[hep-ph\]](#).
  - [5] A. Ali, J. S. Lange, and S. Stone, *Prog. Part. Nucl. Phys.* **97**, 123 (2017), [arXiv:1706.00610 \[hep-ph\]](#).
  - [6] S. L. Olsen, T. Skwarnicki, and D. Zieminska, *Rev. Mod. Phys.* **90**, 015003 (2018), [arXiv:1708.04012 \[hep-ph\]](#).
  - [7] F.-K. Guo, C. Hanhart, U.-G. Meißner, Q. Wang, Q. Zhao, and B.-S. Zou, *Rev. Mod. Phys.* **90**, 015004 (2018), [Erratum: *Rev. Mod. Phys.* 94, 029901 (2022)], [arXiv:1705.00141 \[hep-ph\]](#).
  - [8] R. M. Albuquerque, J. M. Dias, K. P. Khemchandani, A. Martínez Torres, F. S. Navarra, M. Nielsen, and C. M. Zanetti, *J. Phys. G* **46**, 093002 (2019), [arXiv:1812.08207 \[hep-ph\]](#).
  - [9] Y.-R. Liu, H.-X. Chen, W. Chen, X. Liu, and S.-L. Zhu, *Prog. Part. Nucl. Phys.* **107**, 237 (2019), [arXiv:1903.11976 \[hep-ph\]](#).
  - [10] F.-K. Guo, X.-H. Liu, and S. Sakai, *Prog. Part. Nucl. Phys.* **112**, 103757 (2020), [arXiv:1912.07030 \[hep-ph\]](#).

- [11] N. Brambilla, S. Eidelman, C. Hanhart, A. Nefediev, C.-P. Shen, C. E. Thomas, A. Vairo, and C.-Z. Yuan, *Phys. Rept.* **873**, 1 (2020), [arXiv:1907.07583 \[hep-ex\]](#).
- [12] H.-X. Chen, W. Chen, X. Liu, Y.-R. Liu, and S.-L. Zhu, *Rept. Prog. Phys.* **86**, 026201 (2023), [arXiv:2204.02649 \[hep-ph\]](#).
- [13] M. Ablikim *et al.* (BESIII), *Phys. Rev. Lett.* **110**, 252001 (2013), [arXiv:1303.5949 \[hep-ex\]](#).
- [14] Z. Q. Liu *et al.* (Belle), *Phys. Rev. Lett.* **110**, 252002 (2013), [Erratum: *Phys.Rev.Lett.* 111, 019901 (2013)], [arXiv:1304.0121 \[hep-ex\]](#).
- [15] M. Ablikim *et al.* (BESIII), *Phys. Rev. Lett.* **129**, 192002 (2022), [Erratum: *Phys.Rev.Lett.* 130, 159901 (2023)], [arXiv:2202.00621 \[hep-ex\]](#).
- [16] M. Ablikim *et al.* (BESIII), *Phys. Rev. D* **105**, 072002 (2022), [arXiv:2201.09710 \[hep-ex\]](#).
- [17] P. Lacock, C. Michael, P. Boyle, and P. Rowland (UKQCD), *Phys. Rev. D* **54**, 6997 (1996), [arXiv:hep-lat/9605025](#).
- [18] J. J. Dudek, R. G. Edwards, M. J. Peardon, D. G. Richards, and C. E. Thomas, *Phys. Rev. D* **82**, 034508 (2010), [arXiv:1004.4930 \[hep-ph\]](#).
- [19] L. Qiu and Q. Zhao, *Chin. Phys. C* **46**, 051001 (2022), [arXiv:2202.00904 \[hep-ph\]](#).
- [20] H.-X. Chen, N. Su, and S.-L. Zhu, *Chin. Phys. Lett.* **39**, 051201 (2022), [arXiv:2202.04918 \[hep-ph\]](#).
- [21] V. Shastry, C. S. Fischer, and F. Giacosa, *Phys. Lett. B* **834**, 137478 (2022), [arXiv:2203.04327 \[hep-ph\]](#).
- [22] M.-J. Yan, J. M. Dias, A. Guevara, F.-K. Guo, and B.-S. Zou, *Universe* **9**, 109 (2023), [arXiv:2301.04432 \[hep-ph\]](#).
- [23] F. Yang, H. Q. Zhu, and Y. Huang, *Nucl. Phys. A* **1030**, 122571 (2023), [arXiv:2203.06934 \[hep-ph\]](#).
- [24] X.-K. Dong, Y.-H. Lin, and B.-S. Zou, *Sci. China Phys. Mech. Astron.* **65**, 261011 (2022), [arXiv:2202.00863 \[hep-ph\]](#).
- [25] M. Aghasyan *et al.* (COMPASS), *Phys. Rev. D* **98**, 092003 (2018), [arXiv:1802.05913 \[hep-ex\]](#).
- [26] The possible explanation of the  $a_1(1420)$  as a TS effect was first pointed out by Qiang Zhao at the HADRON2013 Conference where the COMPASS result was first reported.
- [27] M. Mikhasenko, B. Ketzer, and A. Sarantsev, *Phys. Rev. D* **91**, 094015 (2015), [arXiv:1501.07023 \[hep-ph\]](#).
- [28] F. Aceti, L. R. Dai, and E. Oset, *Phys. Rev. D* **94**, 096015 (2016), [arXiv:1606.06893 \[hep-ph\]](#).
- [29] G. D. Alexeev *et al.* (COMPASS), *Phys. Rev. Lett.* **127**, 082501 (2021), [arXiv:2006.05342 \[hep-ph\]](#).
- [30] A. Rabusov, D. Greenwald, and S. Paul (Belle), in *20th International Conference on Hadron Spectroscopy and Structure* (2023) [arXiv:2310.09155 \[hep-ex\]](#).
- [31] M. Ablikim *et al.* (BESIII), *Phys. Rev. Lett.* **121**, 022001 (2018), [arXiv:1802.00583 \[hep-ex\]](#).
- [32] H.-J. Jing, S. Sakai, F.-K. Guo, and B.-S. Zou, *Phys. Rev. D* **100**, 114010 (2019), [arXiv:1907.12719 \[hep-ph\]](#).
- [33] M. Ablikim *et al.* (BESIII), (2023), [arXiv:2311.07043 \[hep-ex\]](#).
- [34] L. Roca, E. Oset, and J. Singh, *Phys. Rev. D* **72**, 014002 (2005), [arXiv:hep-ph/0503273](#).
- [35] A. Dobado, M. J. Herrero, and T. N. Truong, *Phys. Lett. B* **235**, 134 (1990).

- [36] N. Kaiser, P. Siegel, and W. Weise, *Nucl. Phys. A* **594**, 325 (1995), [arxiv:nucl-th/9505043](#).
- [37] J. A. Oller and E. Oset, *Nucl. Phys. A* **620**, 438 (1997), [arxiv:hep-ph/9702314](#).
- [38] J. A. Oller and E. Oset, *Phys. Rev. D* **60**, 074023 (1999), [arxiv:hep-ph/9809337](#).
- [39] U.-G. Meissner and J. A. Oller, *Nucl. Phys. A* **673**, 311 (2000), [arxiv:nucl-th/9912026](#).
- [40] S. Navas *et al.* (Particle Data Group), *Phys. Rev. D* **110**, 030001 (2024).
- [41] J. A. Oller and U. G. Meissner, *Phys. Lett. B* **500**, 263 (2001), [arXiv:hep-ph/0011146](#).
- [42] J.-X. Lu, L.-S. Geng, M. Doering, and M. Mai, *Phys. Rev. Lett.* **130**, 071902 (2023), [arXiv:2209.02471 \[hep-ph\]](#).
- [43] X.-K. Dong, F.-K. Guo, and B.-S. Zou, *Phys. Rev. Lett.* **126**, 152001 (2021), [arXiv:2011.14517 \[hep-ph\]](#).
- [44] C. Adolph *et al.* (COMPASS), *Phys. Rev. Lett.* **115**, 082001 (2015), [arXiv:1501.05732 \[hep-ex\]](#).
- [45] A. Kucukarslan and U.-G. Meissner, *Mod. Phys. Lett. A* **21**, 1423 (2006), [arXiv:hep-ph/0603061](#).
- [46] A. J. Woss, C. E. Thomas, J. J. Dudek, R. G. Edwards, and D. J. Wilson, *Phys. Rev. D* **100**, 054506 (2019), [arXiv:1904.04136 \[hep-lat\]](#).
- [47] C. W. Xiao, J. M. Dias, L. R. Dai, W. H. Liang, and E. Oset, (2024), [arXiv:2402.17584 \[hep-ph\]](#).
- [48] M. Ablikim *et al.* (BESIII), *Phys. Rev. D* **99**, 011101 (2019), [arXiv:1801.10384 \[hep-ex\]](#).
- [49] F. Nichitiu *et al.* (OBELIX), *Phys. Lett. B* **545**, 261 (2002).
- [50] M. F. M. Lutz and E. E. Kolomeitsev, *Nucl. Phys. A* **730**, 392 (2004), [arXiv:nucl-th/0307039](#).
- [51] V. R. Debastiani, F. Aceti, W.-H. Liang, and E. Oset, *Phys. Rev. D* **95**, 034015 (2017), [arXiv:1611.05383 \[hep-ph\]](#).
- [52] W.-H. Liang, S. Sakai, J.-J. Xie, and E. Oset, *Chin. Phys. C* **42**, 044101 (2018), [arXiv:1711.04603 \[hep-ph\]](#).
- [53] R. Aaij *et al.* (LHCb), *Phys. Rev. Lett.* **112**, 091802 (2014), [arXiv:1310.2145 \[hep-ex\]](#).
- [54] S. Stone and L. Zhang, *Phys. Rev. Lett.* **111**, 062001 (2013), [arXiv:1305.6554 \[hep-ex\]](#).
- [55] P. G. Ortega, J. Segovia, D. R. Entem, and F. Fernandez, *Phys. Rev. D* **94**, 074037 (2016), [arXiv:1603.07000 \[hep-ph\]](#).
- [56] M. Albaladejo, P. Fernandez-Soler, J. Nieves, and P. G. Ortega, *Eur. Phys. J. C* **78**, 722 (2018), [arXiv:1805.07104 \[hep-ph\]](#).
- [57] M.-J. Yan, X.-H. Liu, S. González-Solís, F.-K. Guo, C. Hanhart, U.-G. Meißner, and B.-S. Zou, *Phys. Rev. D* **98**, 091502 (2018), [arXiv:1805.10972 \[hep-ph\]](#).
- [58] Z. Yang, G.-J. Wang, J.-J. Wu, M. Oka, and S.-L. Zhu, *Phys. Rev. Lett.* **128**, 112001 (2022), [arXiv:2107.04860 \[hep-ph\]](#).
- [59] F.-Z. Peng, M.-J. Yan, and M. Pavon Valderrama, *Phys. Rev. D* **108**, 114001 (2023), [arXiv:2304.13515 \[hep-ph\]](#).
- [60] G.-J. Wang, Z. Yang, J.-J. Wu, M. Oka, and S.-L. Zhu, (2023), [arXiv:2306.12406 \[hep-ph\]](#).
- [61] Y.-b. Shen, Z.-W. Liu, J.-X. Lu, M.-Z. Liu, and L.-S. Geng, (2025), [arXiv:2506.23476 \[hep-ph\]](#).
- [62] L.-L. Wang, X.-M. Zhao, X.-H. Liu, and M.-J. Yan, (2025), [arXiv:2511.19534 \[hep-ph\]](#).
- [63] F.-K. Guo, C. Hanhart, and U.-G. Meissner, *Phys. Lett. B* **665**, 26 (2008), [arXiv:0803.1392 \[hep-ph\]](#).

- [64] F.-K. Guo, C. Hanhart, and U.-G. Meissner, *Phys. Rev. Lett.* **102**, 242004 (2009), [arXiv:0904.3338 \[hep-ph\]](#).
- [65] M. Bayar, W. H. Liang, and E. Oset, *Phys. Rev. D* **90**, 114004 (2014), [arXiv:1408.6920 \[hep-ph\]](#).
- [66] J. Abdallah *et al.* (DELPHI), *Phys. Lett. B* **569**, 129 (2003), [arXiv:hep-ex/0309057](#).
- [67] L. R. Dai, J. Song, and E. Oset, *Phys. Lett. B* **846**, 138200 (2023), [Erratum: *Phys.Lett.B* 864, 139424 (2025)], [arXiv:2306.01607 \[hep-ph\]](#).
- [68] J. Song, L. R. Dai, and E. Oset, *Phys. Rev. D* **108**, 114017 (2023), [arXiv:2307.02382 \[hep-ph\]](#).
- [69] R. Dickson *et al.* (CLAS), *Phys. Rev. C* **93**, 065202 (2016), [arXiv:1604.07425 \[nucl-ex\]](#).
- [70] M. Ablikim *et al.* (BESIII), *Phys. Rev. D* **91**, 052017 (2015), [arXiv:1412.5258 \[hep-ex\]](#).
- [71] R. L. Workman *et al.* (Particle Data Group), *PTEP* **2022**, 083C01 (2022).
- [72] S. Clymton and H.-C. Kim, *Phys. Rev. D* **110**, 114002 (2024), [arXiv:2409.02420 \[hep-ph\]](#).
- [73] M. Ablikim *et al.* (BESIII), *Phys. Rev. D* **91**, 112008 (2015), [arXiv:1503.04699 \[hep-ex\]](#).
- [74] D. Aston *et al.*, *Phys. Lett. B* **201**, 573 (1988).
- [75] A. Abele *et al.* (Crystal Barrel), *Phys. Lett. B* **415**, 280 (1997).
- [76] M. Ablikim *et al.* (BESIII), *Phys. Rev. D* **98**, 072005 (2018), [arXiv:1804.05536 \[hep-ex\]](#).
- [77] L. S. Geng, E. Oset, L. Roca, and J. A. Oller, *Phys. Rev. D* **75**, 014017 (2007), [arXiv:hep-ph/0610217](#).
- [78] J.-M. Xie, J.-X. Lu, L.-S. Geng, and B.-S. Zou, *Phys. Rev. D* **108**, L111502 (2023), [arXiv:2307.11631 \[hep-ph\]](#).
- [79] J.-M. Xie, Z.-W. Liu, J.-X. Lu, H. Liang, R. Molina, and L.-S. Geng, (2025), [arXiv:2511.14380 \[hep-ph\]](#).
- [80] L. Meng, G.-J. Wang, B. Wang, and S.-L. Zhu, *Phys. Rev. D* **104**, 051502 (2021), [arXiv:2107.14784 \[hep-ph\]](#).
- [81] X.-Z. Ling, M.-Z. Liu, L.-S. Geng, E. Wang, and J.-J. Xie, *Phys. Lett. B* **826**, 136897 (2022), [arXiv:2108.00947 \[hep-ph\]](#).
- [82] A. Feijoo, W. H. Liang, and E. Oset, *Phys. Rev. D* **104**, 114015 (2021), [arXiv:2108.02730 \[hep-ph\]](#).
- [83] S. Fleming, R. Hodges, and T. Mehen, *Phys. Rev. D* **104**, 116010 (2021), [arXiv:2109.02188 \[hep-ph\]](#).
- [84] M.-J. Yan and M. P. Valderrama, *Phys. Rev. D* **105**, 014007 (2022), [arXiv:2108.04785 \[hep-ph\]](#).
- [85] H. Ren, F. Wu, and R. Zhu, *Adv. High Energy Phys.* **2022**, 9103031 (2022), [arXiv:2109.02531 \[hep-ph\]](#).
- [86] M.-L. Du, V. Baru, X.-K. Dong, A. Filin, F.-K. Guo, C. Hanhart, A. Nefediev, J. Nieves, and Q. Wang, *Phys. Rev. D* **105**, 014024 (2022), [arXiv:2110.13765 \[hep-ph\]](#).
- [87] M. Albaladejo, *Phys. Lett. B* **829**, 137052 (2022), [arXiv:2110.02944 \[hep-ph\]](#).
- [88] C. Deng and S.-L. Zhu, *Phys. Rev. D* **105**, 054015 (2022), [arXiv:2112.12472 \[hep-ph\]](#).
- [89] M.-J. Yan, F.-Z. Peng, M. Sánchez Sánchez, and M. Pavon Valderrama, *Phys. Rev. D* **104**, 114025 (2021), [arXiv:2102.13058 \[hep-ph\]](#).
- [90] J. Ji, Y. Xing, X. Wu, N. Xu, and Y. Tan, *Chin. Phys. C* **49**, 013101 (2025), [arXiv:2409.08933 \[hep-ph\]](#).
- [91] X. Liu, H. Zheng, D. Chen, H. Huang, and J. Ping, (2025), [arXiv:2505.12828 \[hep-ph\]](#).
- [92] F.-L. Wang, S.-Q. Luo, R.-Q. Qian, and X. Liu, *Phys. Rev. D* **110**, 114041 (2024), [arXiv:2410.15339](#)

[hep-ph].

[93] X.-M. Tang, L.-c. Sheng, Q. Huang, and R. Chen, *Phys. Lett. B* **870**, 139896 (2025), arXiv:2508.15640

[hep-ph].